

## Near-Infrared Classification Spectroscopy: H-band Spectra of Fundamental MK Standards

Michael R. Meyer<sup>1</sup>

Five College Astronomy Department  
University of Massachusetts  
Amherst, MA 01003  
mmeyer@as.arizona.edu

Suzan Edwards

Five College Astronomy Department  
Smith College, Northampton, MA 01063  
edwards@makapuu.ast.smith.edu

Kenneth H. Hinkle

Kitt Peak National Observatory<sup>2</sup>  
National Optical Astronomy Observatories, Tucson, AZ 85721  
hinkle@noao.edu

Stephen E. Strom

Five College Astronomy Department  
University of Massachusetts, Amherst, MA 01003  
sstrom@tsaile.phast.umass.edu

---

<sup>1</sup>Current Address: Hubble Fellow, Steward Observatory, The University of Arizona, 933 N. Cherry Ave., Tucson, AZ 85721-0065

<sup>2</sup>Operated by the Association of Universities for Research in Astronomy, Inc. under cooperative agreement with the National Science Foundation.

## ABSTRACT

We present a catalogue of H-band spectra for 85 stars of approximately solar abundance observed at a resolving power of 3000 with the KPNO Mayall 4m FTS. The atlas covers spectral types O7–M5 and luminosity classes I–V as defined on the MK system. We identify both atomic and molecular indices and line-ratios which are temperature and luminosity sensitive allowing spectral classification to be carried out in the H-band. The line ratios permit spectral classification in the presence of continuum excess emission, which is commonly found in pre-main sequence and evolved stars. We demonstrate that with spectra of  $R = 1000$  obtained at  $SNR > 50$  it is possible to derive spectral types within  $\pm 2$  subclasses for late-type stars. These data are available electronically through the Astronomical Data Center in addition to being served on the World-Wide-Web.

*Subject headings:* infrared: spectroscopy — stars: spectral classification — stars: standards — techniques: spectroscopic

## 1. Introduction

With the recent development of large-format infrared array detectors, high quality photometric surveys are routinely conducted at wavelengths between 1–2.5  $\mu\text{m}$ . Soon the completion of the 2 Micron All-Sky Survey (2MASS; Skrutskie 1997) and DENIS (Epchtein et al. 1997) will provide comprehensive catalogues of near-infrared sources with detection limits sensitive to a wide variety of stellar and non-stellar objects. Infrared spectra will be required for appropriate identification of many of these sources, and for further study of their astrophysical properties.

The pioneering study of Johnson and Mendez (1970) was the first to explore the spectra of a large sample of normal stars in the near-infrared. However many years passed before improvements in instrumentation made possible similar observations of large numbers of targets of astrophysical interest. The majority of the work done in near-infrared spectroscopy to date has been focused on the K-band, in large part because intrinsically cool or heavily obscured objects are typically brighter at K-band than in the J- or H-bands. In 1986, Kleinmann and Hall (1986; KH86) provided the first comprehensive medium resolution atlas ( $R = 3000$ ) of stellar spectra in the K-band, covering all luminosity classes, but restricted to spectral types between F8–M7. More recently, Wallace and Hinkle (1997;

WH97) have extended the KH96 K–band atlas, using the same FTS spectrograph on the KPNO 4m with  $R = 3000$ , but including stellar spectra spanning spectral types O–M and luminosity classes I–V. They also summarize the considerable body of work directed toward K–band spectroscopy in the last decade.

While in many situations, the K–band will be the wavelength selection of choice for spectroscopic studies of highly obscured or very cool objects, the presence of circumstellar dust ( $T_{vap} < 2000K$ ; Pollack et al. 1994) often results in significant excess continuum emission longward of  $2 \mu\text{m}$ . This continuum excess is commonly found in two important classes of objects: young stars with circumstellar disks (e.g. Meyer, Calvet, & Hillenbrand, 1997) and evolved stars with extensive envelopes from mass-loss (e.g. Le Bertre 1997). Near–infrared excess due to warm dust can also complicate spectroscopic studies of composite stellar systems aimed at discerning the stellar populations of other galaxies (e.g. Schinnerer et al. 1997). Continuum excess longward of  $2 \mu\text{m}$  will weaken or even render invisible the photospheric features in the K–band, while the photosphere will dominate at shorter wavelengths. In such a situation, near infrared spectra shortward of  $2 \mu\text{m}$  will be required to see the stellar photosphere too obscured to be detected optically. To date, there has been relatively little work in the H–band ( $1.55\text{--}1.75 \mu\text{m}$ ). Recent publications include: i) observations of 40 G, K, and M stars of luminosity class I and III at  $R = 1500$  by Origlia, Moorwood, and Oliva (1993); ii) the library of 56 spectra O–M of luminosity class I, II, and V at  $R = 500$  (Lancon & Rocca–Volmerange, 1992); iii) a library of 37 stars of luminosity classes I, III, V at  $R = 1500 - 2000$  (Dallier, Boisson, & Joly 1996) over a limited portion of the H–band; and iv) a study of 9 OB Stars at  $R = 570$  (Blum et al. 1997).

Here we present an H–band spectral atlas for 85 stars of nearly solar abundance with spectral types on the MK classification system ranging from 07–M5 and luminosity classes I–V. These  $R = 3000$  spectra were collected with the same FTS at the KPNO 4m as the K–band atlases of KH86 and WH97. In Section 2, we describe the sample selection and in Section 3 we describe the observations and calibration of the data. In Section 4 we discuss the dependence of the spectral features on temperature and luminosity and suggest a two–dimensional classification appropriate for late-type stars. In Section 5 we discuss near–IR spectral classification with regard to wavelength range/spectral resolution, and conclude with a summary of our results.

## 2. Defining the Sample

In our sample selection, we chose optically visible stars which had previously been identified on the temperature and luminosity scales of the revised MK system (Keenan

1987). <sup>3</sup> The majority of the stars were drawn from the following fundamental lists: i) Morgan, Abt, and Tapscott (1978) for 29 stars O6–G0; ii) Keenan and McNeil (1989) for 45 stars G0–K5; and iii) Kirkpatrick, Henry, and McCarthy (1991) for 5 late-type dwarfs K5–M3. We supplemented these primary standards with an additional 5 secondary standards from the compilation of Jaschek, Conde, and de Sierra (1964) and one late-type dwarf classified by Henry, Kirkpatrick, and Simons (1994).

In order to cover as complete a range of stellar temperature and luminosity as possible, we defined a two-dimensional grid with 26 bins of spectral type and three bins of luminosity class. Our temperature grid is binned  $\times 2$  more coarsely in spectral subclass than the revised MK system, so that we typically sample only every other MK subclass. The three luminosity bins are divided into supergiants (I–II), giants (III), and subgiants/dwarf stars (IV–V). A full sampling of this grid would have resulted in 78 distinct temperature/luminosity pairs. Our atlas includes a total of 85 sources with 53 of the bins filled. Grid coverage was finer among the later spectral types, where for stars G0 and later, we filled 26 of the 27 bins (9 spectral types  $\times$  3 luminosity classes). In contrast, for stars earlier than G0, only 27 of the 51 bins were covered (17 spectral types  $\times$  3 luminosity classes).

The 85 individual stars in our H-band survey are listed in Table 1 along with relevant stellar properties taken from the Bright Star Catalogue (Hoffleit & Jaschek 1982). Additional restrictions on the sample selection included: i)  $v \sin i < 250 \text{ km s}^{-1}$  with exception of HR3982 (B7 V); ii) near-solar metallicity (avoiding those MK standards which exhibit spectral peculiarities due to enhanced or deficient metal abundance); and iii) no visual companions within the beam (separations 1 – 5"). Our program was begun in advance of the K-band FTS atlas of WH97, and their sources are drawn in large measure from our sample. We note in Table 1 the stars for which K-band spectra can be found in the WH97 digital atlas.

Table 2 and Figure 1 provide additional insight into the temperature and luminosity coverage of our sample. In Table 2, we list each of the spectral type and luminosity bins we have "filled". For each bin in which there is at least one spectrum, we give the corresponding effective temperature. For most stars, we adopted the temperature scale of Tokunaga (1996), except for giants earlier than G0 where we adopted Schmidt–Kaler (1982) <sup>4</sup>. Figure 1 provides a schematic illustrating the temperature and luminosity

---

<sup>3</sup>For a detailed listing of spectral types and luminosity classes in the revised MK system see Keenan (1985).

<sup>4</sup>Recent work by Bessell, Castelli, and Plez (1998) provides updated temperatures, colors, and bolometric corrections for a wide range of spectral types and luminosity classes.

coverage for the 85 stars in our sample. In this illustration we have applied the same main sequence bolometric corrections to both dwarf (27) and subgiant (11) stars; as such they are indistinguishable in this diagram.

### 3. Observations and Data Calibration

Observations of our 85 sample stars were obtained at the Mayall 4m telescope at Kitt Peak National Observatory during four separate observing runs from 1993–1994 (Table 3). We used the Fourier Transform Spectrometer (FTS) dual-output interferometer (Hall et al. 1979). The FTS was ideal for this program for several reasons. First, the wavelength coverage of the FTS is limited only by the bandpass of the blocking filters, independent of the spectral resolution. This gave us complete coverage in the J- and H-bands which would have been difficult to obtain with available grating spectrographs. For example, our H-band spectral range is a factor of two greater than the spectra of Dallier et al. (1996). Secondly, the spectral resolution is fixed by the path difference scanned with the interferometer so we were able to chose the highest resolution possible and achieve S/N in excess of 75 for the majority of our sources.<sup>5</sup> Finally, because of the novel background subtraction algorithm of the 4m FTS described below, we were able to observe the brightest stars in our sample ( $H < 3.0^m$ ) during good daytime conditions (typically mornings). Combining daytime observations with targeted nighttime observations of key faint sources, the FTS provided a uniform set of high quality spectra for a large sample of spectral standards.

Our observing program included simultaneous spectral coverage in both the J-band and the H-band. However, the J-band data presented difficulties which made it expeditious to focus our initial effort on the H-band. The primary problems with the J-band spectra were; i) the inherent difficulty in data reduction due to rapid temporal variations in telluric water vapor absorption; and ii) and the relative paucity of strong features which would allow spectral classification over the full range of stellar temperature and luminosity. We defer discussion of the J-band spectra to a future contribution.

Spectra were collected simultaneously in the J- and H-bands with the use of a dichroic beamsplitter to separate the wavelengths longward and shortward of  $1.5 \mu\text{m}$ . Each star was centered within an input aperture of 3.8 arcsec while sky background was measured through an identical aperture 50.0 arcsec away. The interferogram was scanned at a rate of 1 kHz as the path difference was varied continuously from 0.0–0.75 cm providing an unapodized

---

<sup>5</sup>For details concerning the advantages and disadvantages of fourier transform spectroscopy, see Bell (1974).

resolution of  $0.8 \text{ cm}^{-1}$ . Data were obtained as separate scan pairs, with the path difference varied first in one direction and then the other. A forward–backward scan pair was treated as an “observation” and observations were repeated in beam–switching mode (A–B–B–A). Because the sky background from each aperture produces an interferogram shifted in phase by  $180^\circ$  at each set of detectors, source spectra are background subtracted in fourier space as they are collected. This permits observations of bright stars to be obtained during good daytime conditions. These beam–switched observations were repeated and scans were averaged until adequate signal–to–noise ratio (SNR) was achieved. The interferograms were transformed at Kitt Peak National Observatory yielding spectra in units of relative flux versus wavenumber ( $\sigma$  in  $\text{cm}^{-1}$ ). The transformed spectra were converted into fits format images and all data reduction was performed using the IRAF software package <sup>6</sup>. The spectra were then convolved with a gaussian filter of half–width  $\delta = 1.2 \text{ cm}^{-1}$ . This procedure, commonly referred to as apodization, eliminates “ringing” observed in the FTS spectra due to the finite scan path of the interferometer. The resulting apodized resolution (Rayleigh criterion) was  $\delta\sigma = 2.1 \text{ cm}^{-1}$  giving a mean resolving power of  $R = 3000$  in the H–band. At this stage the J– and H–band spectra were separated for ease of reduction. The slope of the continuum was normalized to 1.0 using a four–segment spline fitting function. Care was taken to keep the residuals from this fit to within 1 %.

Next we corrected the spectra for telluric absorption features present in the spectra which varied with zenith angle. We attempted to construct an opacity map for the earth’s atmosphere by dividing normalized spectra obtained of the A0 star standards at different airmass. Because of the simplicity of the A0 star spectra, showing primarily hydrogen lines in absorption, it was relatively easy to monitor the degree to which this procedure was successful. In dividing two normalized spectra of the same star taken at different airmass, all stellar photospheric absorption features should directly cancel, leaving only those absorption features due to the earth’s atmosphere. If we assume that the opacity of the telluric absorption is directly proportional to airmass we derive:

$$\tau(\sigma, X = 1.0) = \frac{1}{(X_{high} - X_{low})} \times \ln\left[\frac{I(\sigma, X_{low})}{I(\sigma, X_{high})}\right] \quad (1)$$

where  $\tau$  is the atmospheric opacity,  $X_{low}$  is the low airmass value, and  $X_{high}$  is the high airmass value. A typical opacity map derived in this way for the H–band is shown in Figure 2. Several of the features in this map identified with known constituents of the earth’s atmosphere such as water vapor, methane, and carbon dioxide, are denoted in

---

<sup>6</sup>IRAF is distributed by the National Optical Astronomy Observatories, which is operated by the Association of Universities for Research in Astronomy, Inc., under contract to the National Science Foundation.

Figure 2. Again if the atmospheric opacity varies linearly with airmass we can simply scale the opacity for each star so that  $\tau(\sigma, X) = X \times \tau(\sigma, X = 1.0)$ . Using this technique we corrected the spectra to zero-airmass;

$$I(\sigma, X = 0.0) = I(\sigma, X) \times e^{\tau(\sigma, X)} \quad (2)$$

We used the highest signal-to-noise A0 standard star spectra ( $SNR > 100$ ) with the largest  $\Delta X$  to define the opacity. We found some residual telluric absorptions, possibly due to water vapor which do not vary strictly with airmass. Such features severely complicate the reduction of the J-band spectra.

Finally, the forward and backward scans of each star were averaged and residuals of the differenced spectra were calculated in order to evaluate the average SNR. The observations were obtained with the goal of achieving SNR of 75 or greater. In most cases this was achieved with the highest quality spectra reaching values of several hundreds. The average SNR for each stellar spectrum is included in Table 5 –Table 8 below.

#### 4. Line Identification and Dependence on Temperature and Luminosity

Representative H-band spectra are shown in Figures 3– 6 for luminosity classes I–II, III, IV, and V, with prominent atomic and molecular features identified. Line identifications were made for the strongest lines from comparison with the solar photospheric and umbral near infrared atlases (Livingston & Wallace 1991 (LW91); Wallace & Livingston 1992 (WL92)). However, at our moderate spectral resolution many features are blended and we found the model atmosphere calculations of Oliva, Moorwood, and Origlia (1993) to be useful in identifying the dominant contributors to a blend in late-type stars.

Visual inspection of the features in Figures 3– 6 reveals that  $R = 3000$  H-band spectra contain sufficient temperature and luminosity sensitive features to enable spectral classes to be distinguished. Beginning with the early type stars, the dominant spectral features are HeI  $5882 \text{ cm}^{-1}$  ( $1.700 \mu\text{m}$ ) and the Brackett series of hydrogen from lines 4-10 ( $1.736 \mu\text{m}$ ) to 4-16 ( $1.556 \mu\text{m}$ ). The He I line exceeds the strength of the Brackett lines in the very earliest stars (O6 to B0), with a maximum equivalent width of  $\sim 0.83 \text{ cm}^{-1}$  (HR1903; B0 Ia), and recedes to undetectable levels ( $\sim 0.10 \text{ cm}^{-1}$ ) by spectral type B8. From the late B to early F stars, the Brackett series dominates the spectrum, after which lines of neutral atomic metals begin to take prominence. The strongest metallic lines include MgI, SiI, CaI, AlI, and FeI, which increase in strength toward the K stars. Finally molecular features of OH and CO dominate the spectra of the latest-type stars from K5–M5. The most striking luminosity-sensitive feature is the second-overtone CO bandhead [ $v, v' = 6, 3$ ] at  $6177 \text{ cm}^{-1}$

(1.619  $\mu\text{m}$ ), which is found in the spectra of the K and M stars. This feature is significantly stronger in stars of lower surface gravity at equivalent spectral type.

To further enable spectral classification in the H-band, we have identified a set of 9 features which are prominent in stars of spectral type A-M. These include a relatively isolated Brackett line (H4-11), 5 neutral metals, and 3 molecular bands. In Table 4, we define 9 narrow band indices with bandpasses ranging from 10 to 50  $\text{cm}^{-1}$ , which include each of these features. The variable widths of the bandpasses were selected to minimize line blending, contamination from residual telluric absorption, and sensitivity to radial velocity shifts. Table 4 also identifies the wavenumber of the dominant contributor and the lower state energy level, the central wavenumber and passband of the index, and additional species which may contribute to the index strength. The equivalent widths of these 9 indices were evaluated from the normalized spectra of our 85 survey stars, and are tabulated in Tables 5 to 8 in units of  $\text{cm}^{-1}$ <sup>7</sup>. Uncertainties in these equivalent widths depend on the SNR of the spectrum in question and the bandpass/strength of the feature. Errors range from  $\sigma_{EW} = 0.02 - 0.1 \text{ cm}^{-1}$  exceeding this upper limit in very few cases. Multiple observations of several sources are listed for comparison.

The temperature and luminosity dependence for four representative indices is illustrated in Figure 7. The 4–11 Brackett line (HI5950) behaves as expected, with a rapid rise to a maximum (at a peak equivalent width of  $\sim 3 \text{ cm}^{-1}$ ) as  $T_{eff}$  approaches 10000 K, and a slower decline toward higher temperatures. The behavior of the index is similar in both the dwarfs and the giants, although the luminosity class I/II sources show a larger scatter, presumably due to intrinsic variability (e.g. Kaufer et al. 1996). The general behavior of the neutral atomic features is illustrated by the Mg6345 index. In luminosity classes IV–V, this index reaches a maximum strength between 5000-6000 K, with a peak equivalent width of  $\sim 2.5 \text{ cm}^{-1}$ . In contrast, the maximum strength of this index in the lower surface gravity objects (also  $\sim 2.5 \text{ cm}^{-1}$ ) is found in the coolest stars in our sample, monotonically decreasing toward higher temperatures; as expected given the behavior of ionization state as a function of surface gravity. The two SiII indices exhibit similar behavior, but the AlII index, (not shown) turns over at much lower temperatures in our dwarf stars because of its lower ionization potential. Note that we have chosen not to form an index based on the strongest SiII line at 6292  $\text{cm}^{-1}$  (1.5892  $\mu\text{m}$ ) because it is coincident with the 4–14 Brackett line of HI at 6297  $\text{cm}^{-1}$  (1.5881  $\mu\text{m}$ ).

The behavior of the molecular features is illustrated for both the second-overtone  $^{12}\text{CO}$  (6,3) and the OH ( $\Delta v = 2$ ) indices. Both indices exhibit a similar behavior with

---

<sup>7</sup>The conversion to angstroms is  $EW(\text{\AA}) = [EW(\text{cm}^{-1})/\sigma^2] \times 10^8$



temperature and luminosity, becoming detectable around  $T_{eff} = 5000$ , with a strength in the giants approximately twice that in the dwarfs. Similar behavior was noted by KH86 in the first-overtone CO features in the K-band. In dwarf stars the second-overtone CO index reaches a maximum before M5, and displays a turnover toward the coolest stars. This may be due in part to features of CaI and FeI which contaminate the index for intermediate spectral types (F5–K3). Ali et al. (1995) find that the relationship between  $T_{eff}$  and equivalent widths of the first-overtone CO bandheads flatten out between 3500–5000 K in dwarf stars. From high resolution ( $R > 45,000$ ) FTS spectra, Wallace & Hinkle (1996) observed that the  $2 \mu\text{m}$  continuum in late-type dwarf stars is suppressed by numerous water vapor features which are blended at intermediate to low resolution. Predicting the equivalent widths of features where the apparent continuum is subject to temperature and luminosity effects is not straight-forward. In contrast, both the CO and OH indices continue to rise at the coolest temperatures for stars of higher luminosity. However, the magnitude (and temperature) of the maximum in the dwarf stars differs between the CO and OH indices, which we use in the next section to define a two-dimensional classification scheme for late-type stars. We note that the OH index begins to include a contribution from the stark-broadened 4-11 Brackett line at  $5949 \text{ cm}^{-1}$  creating a secondary maximum in the strength of this index around 10,000 K in the dwarf stars.

While the temperature and luminosity dependence of the atomic features is readily understood through application of the Saha and Boltzman equations governing the population of the ionization states and energy levels respectively, the explanation behind the behavior of the molecular features is more subtle. Two possibilities for the factor of two enhancement in the molecular bands in the giants over the dwarfs have been explored in the literature. One attributes the luminosity dependence in the molecular features to differing microturbulence in the atmospheres of dwarfs and giants. The expectation is that larger microturbulence in the lower surface gravity giants effectively broadens the opacity of the feature over a larger frequency interval in these saturated features, thereby enhancing the equivalent width (McWilliams & Lambert 1984). Another possible contributor is the differing depth of the line formation region in the dwarfs versus the giants, which is fixed by the  $\text{H}^-$  opacity. As described by Gray (1992) higher surface gravity results in a higher electron pressure (and thus  $\text{H}^-$  column density). This brings the CO line formation region closer to the stellar surface reducing  $N_{CO}$  according to the following proportionality:

$$P_e \sim g^{1/3} \sim N_{H^-} \sim 1/N_{CO} \quad (3)$$

In any case, this luminosity dependence of the band strength gives an excellent empirical discriminant between giants and dwarfs, which we exploit below to develop a two dimensional spectral index.

To discern surface gravity effects between the super-giants and giants or between sub-giants and dwarf stars requires more careful study. A detailed examination of line strengths as a function of surface gravity at a fixed temperature reveal the expected trends. However, this behavior does not reveal itself in the coarse analysis afforded by our narrow-band indices.

While the temperature and luminosity sensitivities outlined above can provide good spectral classification in many instances, discriminants which do not rely on absolute line strength are required when a star is subject to near-infrared continuum veiling. In this case line ratio diagnostics are to be preferred, since absorption features will appear shallower in the presence of continuum excess but line ratios will be preserved as long as the excess is not strongly wavelength dependent. We have identified one diagnostic based on line ratios which can be used to evaluate both temperature and luminosity for stars from K3-M5 in the presence of continuum veiling. This two-dimensional spectral index is defined as:

$$\frac{EW[OH5920]}{EW[Mg6345]} \text{ vs. } \frac{EW[CO6018 + CO6170]}{EW[Mg6345]} \quad (4)$$

where EW is the equivalent width in  $\text{cm}^{-1}$  for the indices identified in Table 4 and listed in Tables 5– 8. The temperature and luminosity dependence of this diagnostic is illustrated in Figure 8. In this diagnostic, the ratio of the OH5920 to Mg6345 indices is temperature sensitive, with distinct temperature dependences for dwarfs and giants. Specifically we find

$$T_{eff}(V) = 4640 \pm 250 - (2610 \pm 110) \frac{EW[OH5920]}{EW[Mg6345]} \quad (5)$$

and

$$T_{eff}(III) = 5100 \pm 180 - (2730 \pm 80) \times \frac{EW[OH5920]}{EW[Mg6345]} \quad (6)$$

The comparison of this temperature sensitive ratio with the sum of the two  $^{12}\text{CO}$  indices, also normalized to Mg6345, then provides an excellent means of identifying both the temperature and luminosity class of late-type stars. Formal errors in the equivalent width suggest that spectral types can be evaluated to within  $\pm 2$  subclasses ( $\pm 300$  K) from K3–M5 using spectra with  $SNR > 50$  based on these indices alone.

## 5. Discussion and Summary

Spectral classification in the near-infrared will become increasingly important in the next decade, as the 2MASS and DENIS near-infrared sky surveys reveal unprecedented numbers of stars which are optically-invisible. Because the 1–2.5  $\mu\text{m}$  region is on the Rayleigh–Jeans tail of most stellar SEDs, it is not an ideal wavelength regime to pursue spectral classification. Yet, there are sufficient features in both the H– and the K–bands to allow most stellar photospheres to be classified. For heavily reddened sources, the K–band will be the wavelength of choice. However, continuum emission from circumstellar dust with temperatures less than 2000 K can heavily veil stellar photospheres at wavelengths greater than 2.0  $\mu\text{m}$ . In this case, shorter wavelength spectra are required in order to identify the underlying star.

The early-type stars are probably the most challenging for spectral classification in the near-infrared. We find that a rough classification from O7–B8 can be made in the H–band by the relative strengths of HeI 5882  $\text{cm}^{-1}$  and the Brackett series (see also Blum et al. 1997). Hanson, Conti, and Rieke (1995) have established a classification scheme in the K–band for O–B stars relying on lines of helium as well as higher ionization species obtained at  $R > 1000$ . For stars A through early K, the H–band may be superior to the K band in providing a large number of intermediate ionization potential species with strong features such as MgI, SiI, and FeI in addition to the numerous Brackett series features. Stars K3–M5 are probably best classified in the K–band (KH86; Ali et al. 1995; WH97) using atomic features of MgI, CaI, and NaI as well as the first–overtone CO bandheads observed at  $R \sim 1000$ . However we have found that these stars also have strong temperature and luminosity sensitive features in the H–band such as MgI, AlI, OH, and the second–overtone CO bandheads. The very latest–type stars ( $> M5$ ) have very strong, broad, molecular features which can be identified at resolutions as low as  $R \sim 300$ . Kirkpatrick et al. 1993 (see also Jones et al. 1996) have classified stars in the I– or the J–band employing features due to VO, TiO, and FeH. In addition, broad water vapor bands observed throughout the 1–2.5  $\mu\text{m}$  region (Jones et al. 1995) are an important opacity source in the atmospheres of the coolest stars as well as brown dwarfs (Allard & Hauschildt 1995). While the I– or J–bands are probably the best spectral regions to classify extremely cool stars (as they lie on the Wien side of the Planck function for these objects) more heavily obscured objects can still be profitably observed at low resolution in the J– and H–bands (e.g. NICMOS on HST) or in the K–band (Wilking, Greene, & Meyer 1998) in search of these water vapor absorptions.

The H–band spectral atlas we have presented is comprised of moderate resolution spectra with  $R \sim 3000$ . In contrast, most spectral classification is typically carried out

with  $R \sim 500 - 1000$ . The strongest and broadest features in the H-band are the CO(6-3) bands and the Brackett lines. These features could be identified with much lower spectral resolution than our survey, at  $R \sim 500$ . The most crowded region in the H-band spectra is that in the vicinity of the HI line at  $5948.50 \text{ cm}^{-1}$  ( $1.68110 \text{ }\mu\text{m}$ ), the AlI triplet at  $5964\text{--}5980 \text{ cm}^{-1}$  ( $1.677\text{--}1.672 \text{ }\mu\text{m}$ ), and the SiI line at  $5993.29 \text{ cm}^{-1}$  ( $1.66853 \text{ }\mu\text{m}$ ). In order to properly separate these important features from each other, a resolving power of  $R \sim 1000$  is required. At this resolution, one can also obtain measurements of the HeI line at  $5882 \text{ cm}^{-1}$  ( $1.700 \text{ }\mu\text{m}$ ). At  $R = 3000$  one can resolve individual components of the AlI triplet, the Mg I doublet, and the CO bandheads, as well as the stark-broadened Brackett lines in the early-type dwarf stars (Table 4). An additional issue in the near-infrared is the significant contribution to shot-noise from air-glow lines. In the H-band air-glow from OH is sufficiently bright and variable that they compromise  $R = 1000$  H-band spectral classification for very faint sources. Spectral resolution as high as  $R \sim 5000$  will be required to resolve the bulk of these air-glow features and to obtain adequate SNR spectra of faint objects <sup>8</sup>.

In summary, we present an H-band spectral atlas at a resolving power of  $R = 3000$  that spans a wide range in stellar temperature (O7-M5) and luminosity class (I-V). This spectral region contains a number of temperature and/or luminosity sensitive atomic and molecular features which will allow spectral classification to be carried out in the H-band. As an example of the efficacy of this spectral range for distinguishing stellar spectral types, we define a set of narrow-band indices which, with  $SNR \sim 50$ , permit classification of late-type stars on the MK system within  $\pm 2$  subclasses. It appears however, that for most applications obtaining H-band spectra at  $R \sim 1000$  will be sufficient for classification.

## 6. Appendix A: Electronic Availability of the Data

The final reduced averaged spectra as well as the difference of the forward and backward scan pairs (see Section 3 for description of the reduction procedure) are available through the Astronomical Data Center (ADC) for each observation listed in this paper. The ADC can be contacted directly: i) by post at Astronomical Data Center, NASA Goddard Space Flight Center, Code 631, Greenbelt, MD 20771; or ii) by telephone at (301) 286-8310; or iii) by fax at (301) 286-1771; or iv) via the internet at <http://adc.gsfc.nasa.gov>. The data are in fits format with pertinent header information included for each image. These fits format files, useful plotting routines, and other relevant information are also available on the World

---

<sup>8</sup> See Herbst (1994) for a comprehensive discussion of OH airglow background suppression strategies.

Wide Web at <http://donald.phast.umass.edu>. The raw FTS data are also available directly from NOAO (contact KHH for details).

We would like to thank Lori Allen, Ed Chang, Lynne Hillenbrand, Susan Kleinmann, Michael Skrutskie, and Lloyd Wallace for helpful discussions. Special thanks to John Carpenter for assisting in the initial compilation of the standard star lists, and to Karen Strom and Stephen Friedman for their assistance in making the data available electronically. Antonella Romano provided assistance in preparing the tables and figures for publication. Support for MRM during the final stages of this work was provided by NASA through Hubble Fellowship grant # HF-01098.01-97A awarded by the Space Telescope Science Institute, which is operated by the Association of Universities for Research in Astronomy, Inc., for NASA under contract NAS 5-26555. SE acknowledges support from the National Science Foundation's Faculty Award for Women Program. This work was supported in part through a grant from the National Science Foundation (# AST-9114863) to SES.

## REFERENCES

- Ali, B., Carr, J.S., DePoy, D.L., Frogel, J.A., & Sellgren, K. 1995, *AJ*, 110, 2415
- Allard, F., & Hausschildt, P.H. 1995, *ApJ*, 445, 433
- Bell, J.R. 1974, *Fourier Transform Spectroscopy*, (John Willey and Sons: New York)
- Bessell, M.S., Castelli, F., & Plez, B. 1998, *A&A*, 333, 231
- Blum, R.D., Ramond, T.M., Conti, P.S., Figer, D.F., & Sellgren, K. 1997, *AJ*, 113, 1855
- Coxon, G. 1965, *Ark. Fys.*, 28, 381
- Dallier, R., Boisson, C., & Joly, M. 1996, *A&ASS*, 116, 239
- Epchtein, N. et al. 1997, *Impact of Large Scale Near-IR Sky Surveys*, eds. Gorzon, F., Epchtein, N., Omont, A., Burton, B., & Persi, P. (Kluwer: Amsterdam, Netherlands)
- Eriksson, K.B.S., & Isberg, H.B.S. 1963, *Ark. Fys.*, 23, 527
- Garcia, J.D., & Mack, J.E. 1965, *JOSA*, 55, 654
- George, T., Urban, W., & LeFloch, A. 1994, *J. Mol. Spec.*, 165, 50
- Gray, D.F. 1992, *The Observation and Analysis of Stellar Photospheres*, (Cambridge University Press: Cambridge), p. 374
- Hall, D.N.B, Ridgeway, S., Bell, E., & Yarborough, J.M. 1979, *Proc. SPIE*, 248, 898
- Hanson, M., Conti, P., & Rieke, M. 1996, *ApJS*, 107, 281

- Henry, T.J., Kirkpatrick, J.D., & Simons, D. 1994, *AJ*, 108, 1437
- Herbst, T.M. 1994, *PASP*, 106, 1298
- Hoffleit, D., & Jaschek, C. 1982, *The Bright Star Catalogue*, Yale Observatory
- Jaschek, C., Conde, H., & de Sierra, A.C. 1964, *La Plata Observatory Bulletin*, 28
- Johnson, H.L., & Mendez, M.E. 1970, *AJ*, 75, 785.
- Jones, H.R.A., Longmore, A.J., Allard, F., Hauschildt, P.H., Miller, S., & Tennyson, J. 1995, *MNRAS*, 277, 767
- Jones, H.R.A., Longmore, A.J., Allard, F., & Hauschildt, P.H. 1996, *MNRAS*, 280, 77
- Kaufer, A. et al. 1997, *A&A*, 320, 273
- Keenan, P.C., 1985, *IAU*, 111, 123
- Keenan, P.C., 1987, *PASP*, 99, 713
- Keenan, P.C., & McNeil, R. 1989, *APJS*, 71, 245
- Kirkpatrick, J.D., Henry, T.J., & McCarthy, D.W. Jr. 1991, *APJS*, 77, 417
- Kirkpatrick, J.D., Kelly, D.M., Rieke, G.H., Liebert, J., Allard, F., Wehrse, R. 1993, *ApJ*, 402, 643
- Kleinmann, S.G., & Hall, D.N.B. 1986, *APJS*, 62, 501 (KH86)
- Koornneef, J. 1983, *A&A*, 128, 84
- Lancon, A., & Rocca-Volmerange, B. 1992, *A&AS*, 96, 593
- Le Bertre, T. 1997, *A&A*, 324, 1059
- Litzen, U. 1964, *Ark. Fys.*, 28, 239
- Livingston, W., & Wallace, L. 1991, *Solar Atlas 1–5  $\mu$ m*, Kitt Peak Observatory Bulletin (LW91)
- McWilliam, A., & Lamber, D.L. 1984, *PASP*, 96, 882
- Meyer, M.R., Calvet, N., & Hillenbrand, L.A. 1997, *AJ*, 114, 288
- Morgan, W., Abt, H., & Tabscott, J. 1978, *Revised MK Spectral Atlas for Stars Ealier than the Sun*, Yerkes and Kitt Peak Observatories
- Origlia, L., Moorwood, A., & Oliva, E. 1993, *A&A*, 280, 536
- Pollack, J.B., Hollenbach, D., Beckwith, S.V.W., Damon, P., Rousch, T., & Fong, W. 1994, *ApJ*, 421, 615.
- Risberg, G. 1965, *Ark. Fys.*, 28, 381

- Schinnerer, E., Eckart, A., Quirrenbach, A., Boker, T., Tacconi–Garman, L.E., Downes, D. 1997, *ApJ*, 488, 174
- Skrutskie, M.F. 1997, *Impact of Large Scale Near-IR Sky Surveys*, eds. Gorzon, F., Epchtein, N., Omont, A., Burton, B., & Persi, P. (Kluwer: Amsterdam, Netherlands)
- Schmidt–Kaler, T.H. 1982, *Physical Parameters of Stars*, Landolt-Bornstein New Series, Vol. 2b, *Astronomy and Astrophysics, Stars and Star Clusters*, ed. K. Shaifers & H. H. Voigt, (Springer–Verlag: New York)
- Tokunaga, A., 1996, *Astrophysical Quantities*, submitted
- Wallace, L., & Livingston, W. 1992, *Atlas of Dark Sunspot Spectrum 1–5  $\mu\text{m}$* , Kitt Peak Observatory Bulletin (WL92)
- Wallace, L. & Hinkle, K. 1996, *APJS*, 107, 312
- Wallace, L. & Hinkle, K. 1997, *APJS*, 111, 445 (WH97)
- Wilking, B.A., Greene, T.P., & Meyer, M.R. 1998, *AJ*, submitted

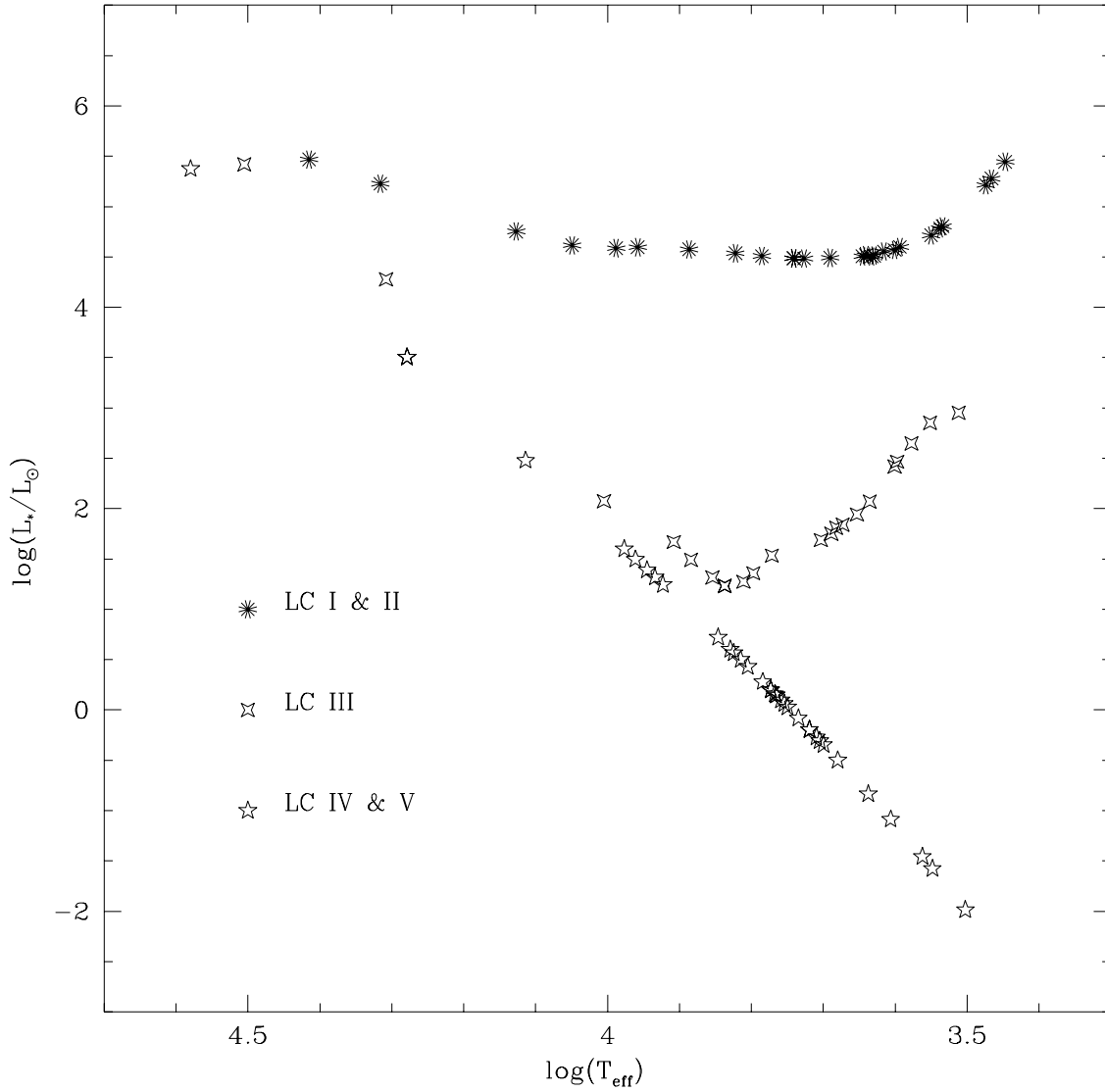


Fig. 1.— Each star in our survey was transformed into the  $L_*$  vs.  $T_{eff}$  plane from the  $V$  magnitude listed in the Bright Star Catalog (Hoffleit & Jaschek 1982), the spectral type–temperature calibration in Table 2, and bolometric corrections for luminosity class I (applied to I–II), III, and V stars (applied to IV–V).



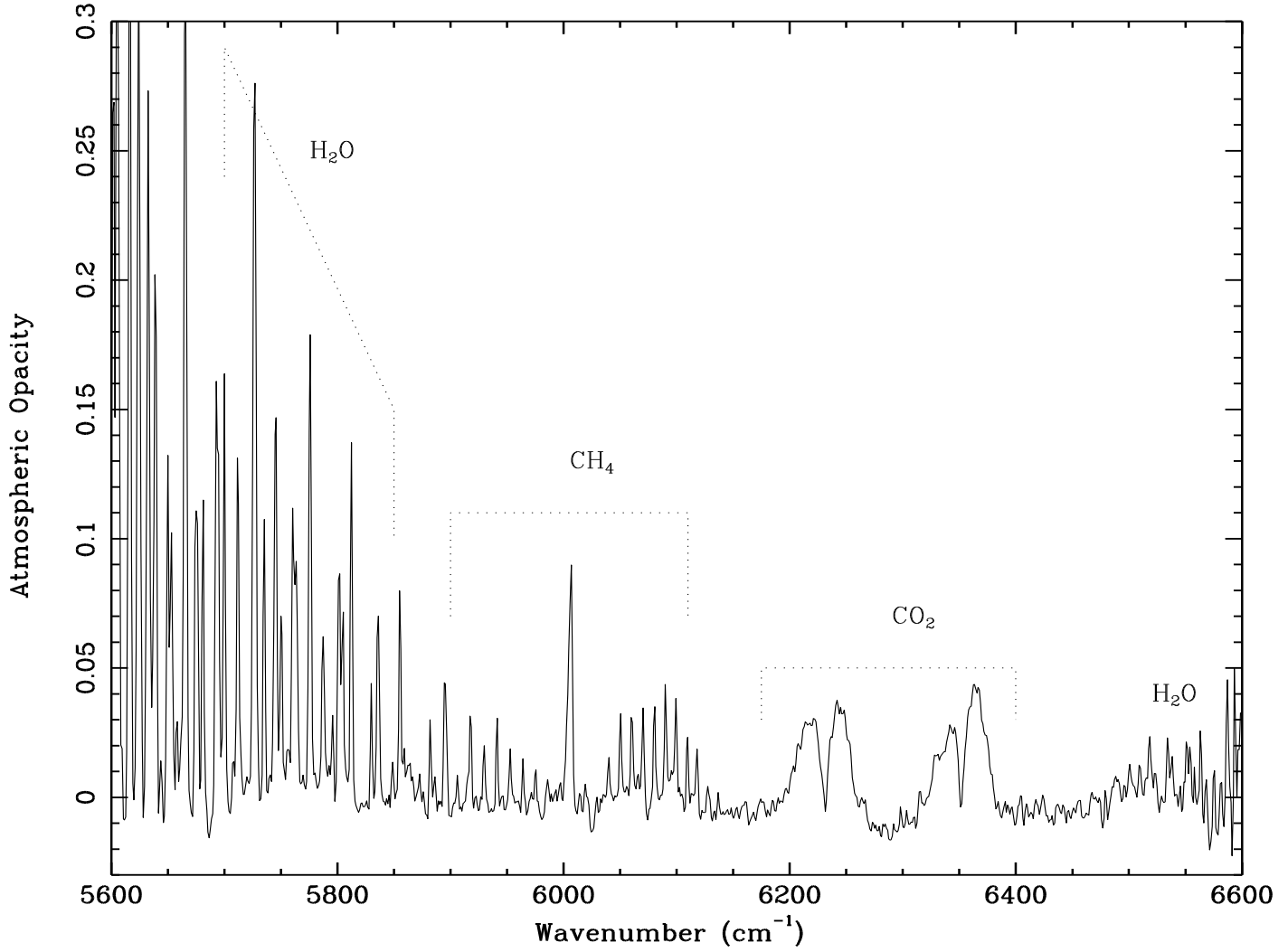


Fig. 2.— Atmospheric opacity in the H-band at a resolving power of  $R = 3000$ . The opacity was derived from ratios of high signal-to-noise spectra of the same star observed at different airmass as discussed in the text.

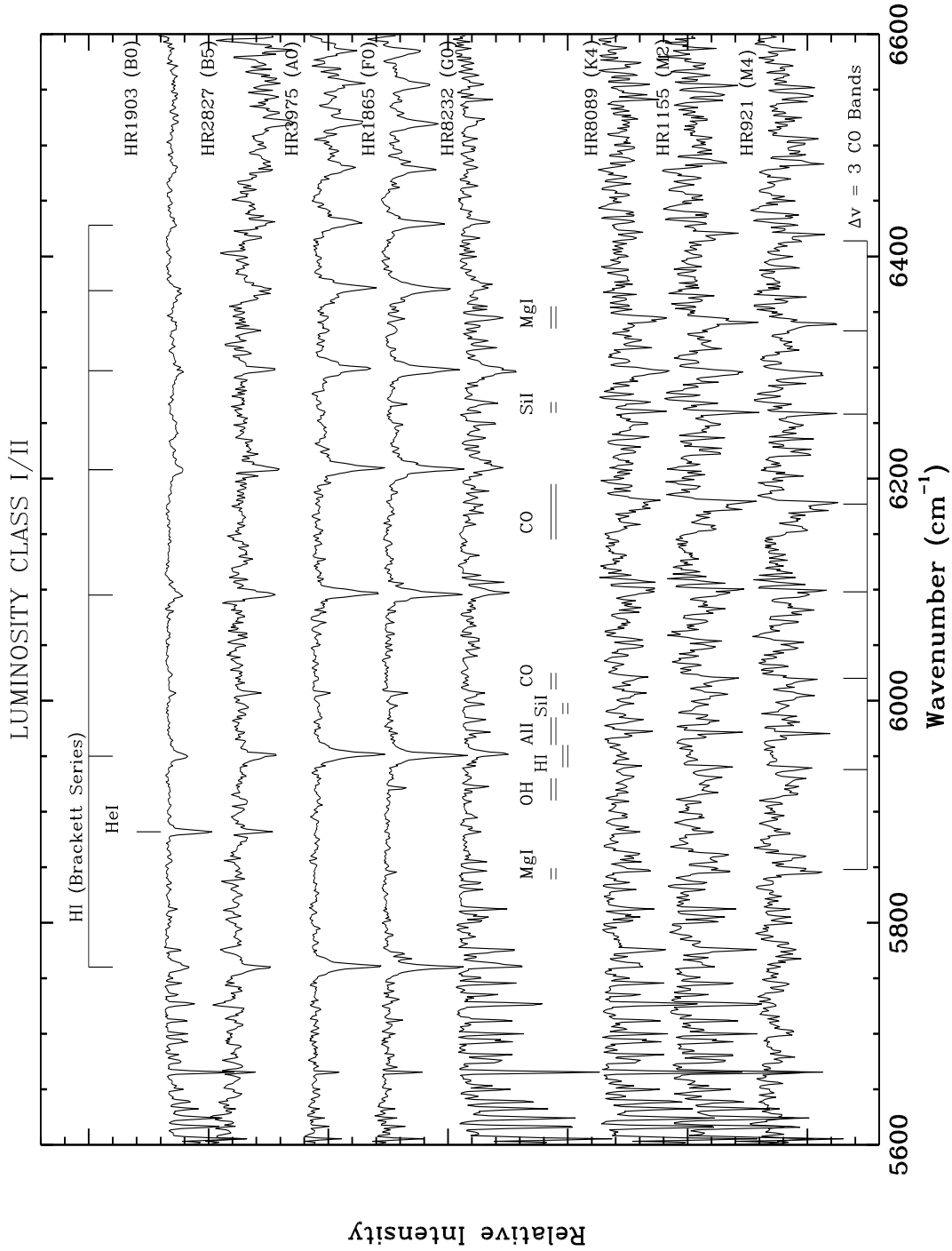


Fig. 3.— Representative H-band spectra of the MK standards plotted as a function of effective temperature from high (top) to low (bottom) for luminosity class I–II stars. Prominent features are indicated, including the indices listed in Table 4.

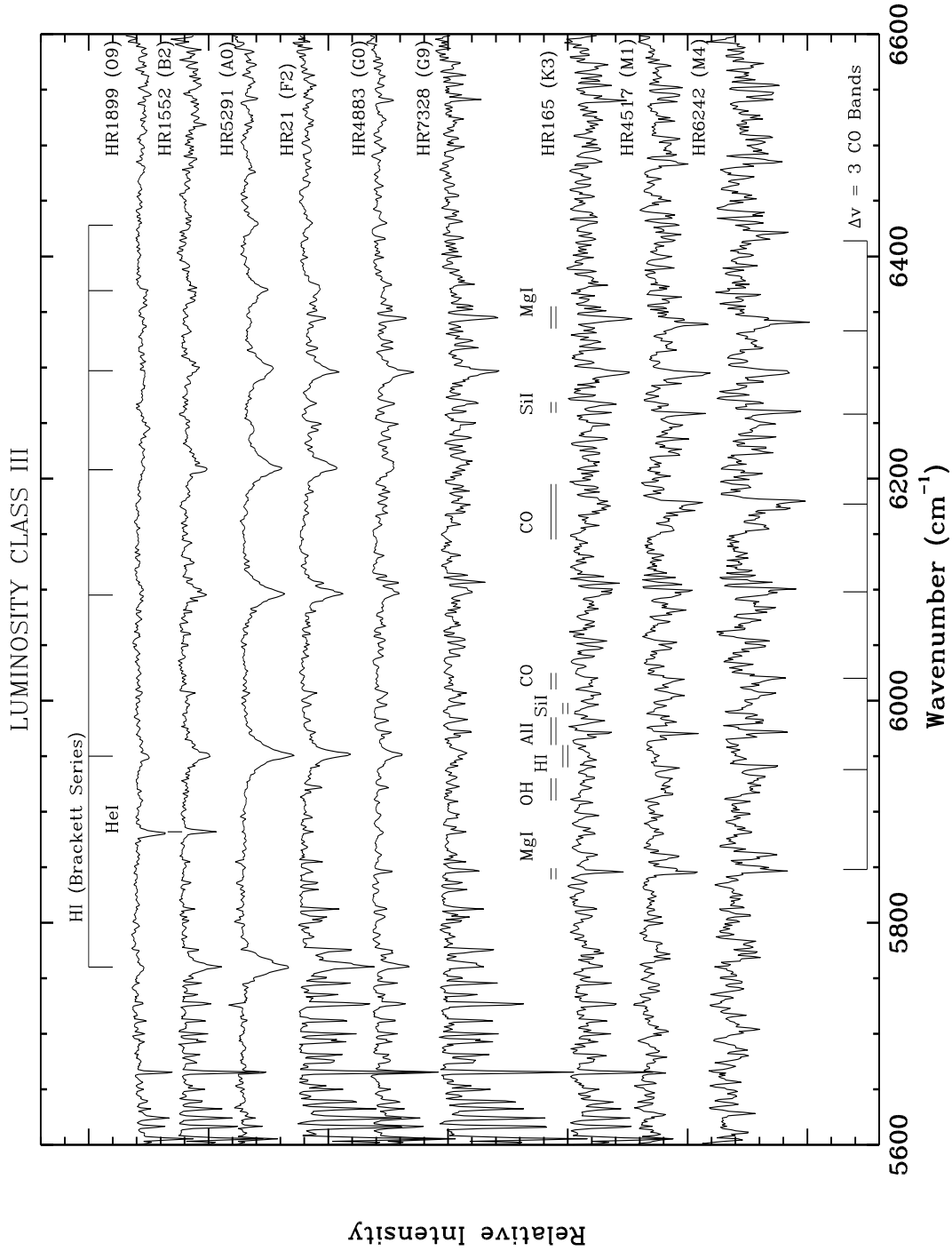


Fig. 4.— Representative H-band spectra of the MK standards plotted as a function of effective temperature from high (top) to low (bottom) for luminosity class III stars. Prominent features are indicated, including the indices listed in Table 4.

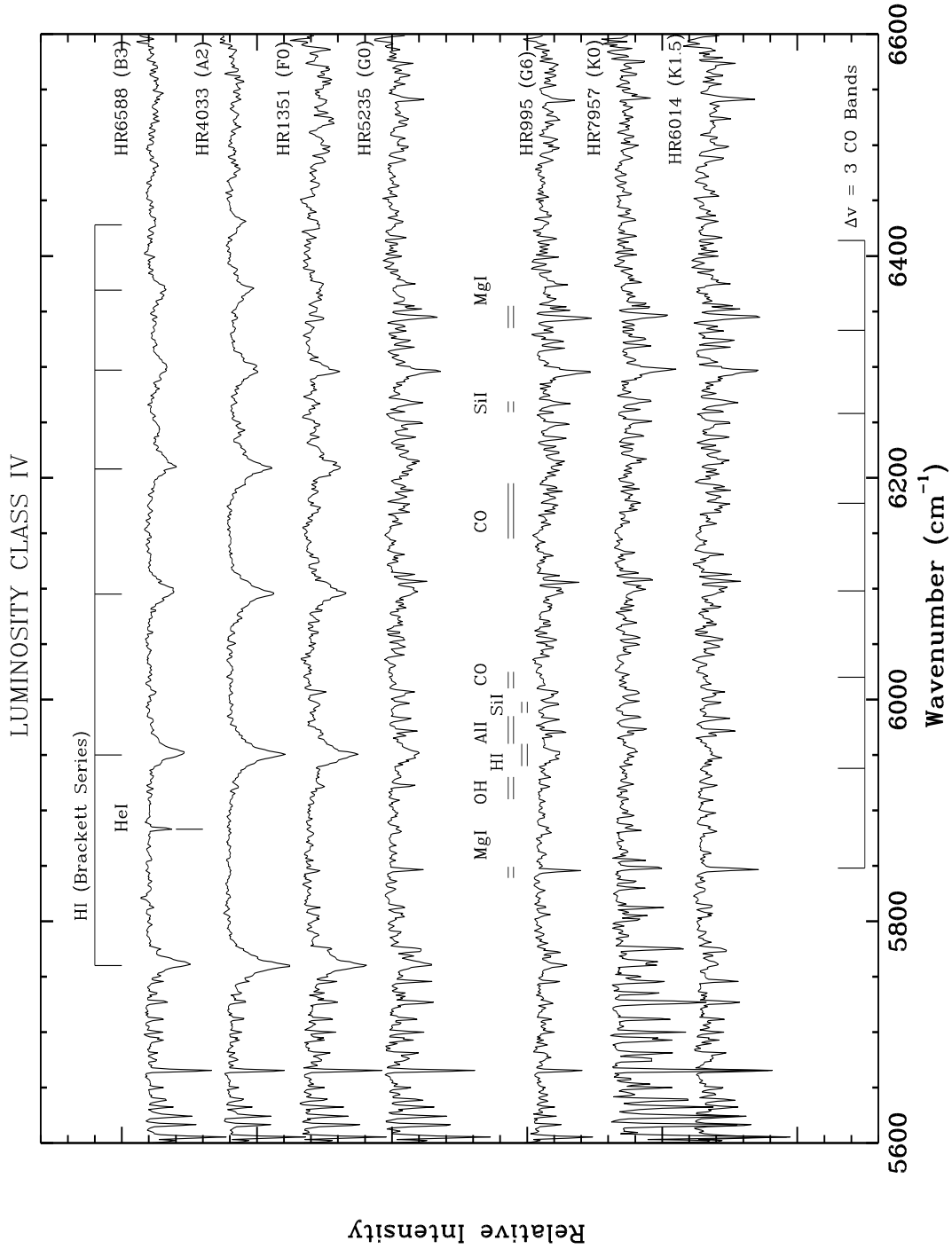


Fig. 5.— Representative H-band spectra of the MK standards plotted as a function of effective temperature from high (top) to low (bottom) for luminosity class IV stars. Prominent features are indicated, including the indices listed in Table 4.

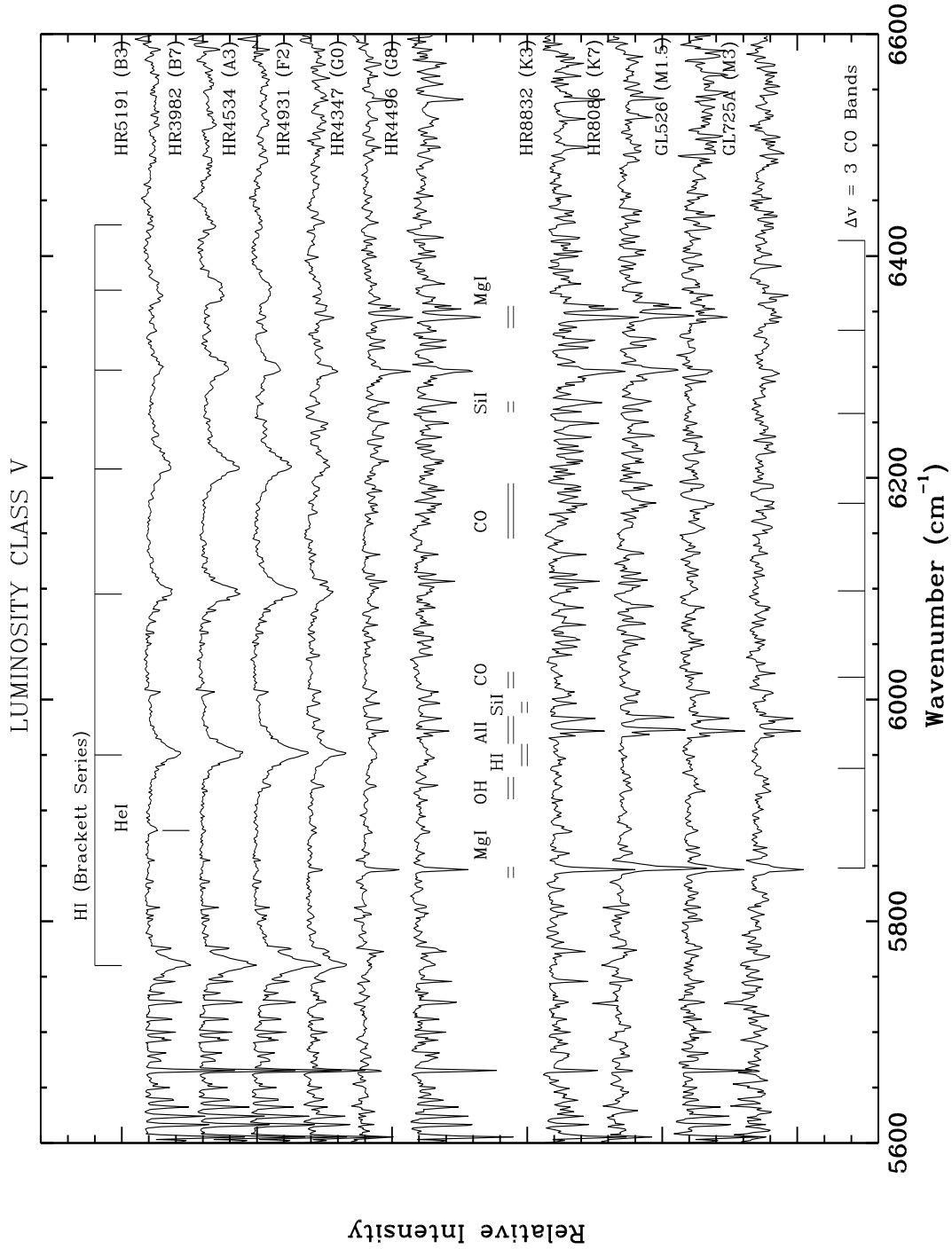


Fig. 6.— Representative H-band spectra of the MK standards plotted as a function of effective temperature from high (top) to low (bottom) for luminosity class V stars. Prominent features are indicated, including the indices listed in Table 4.

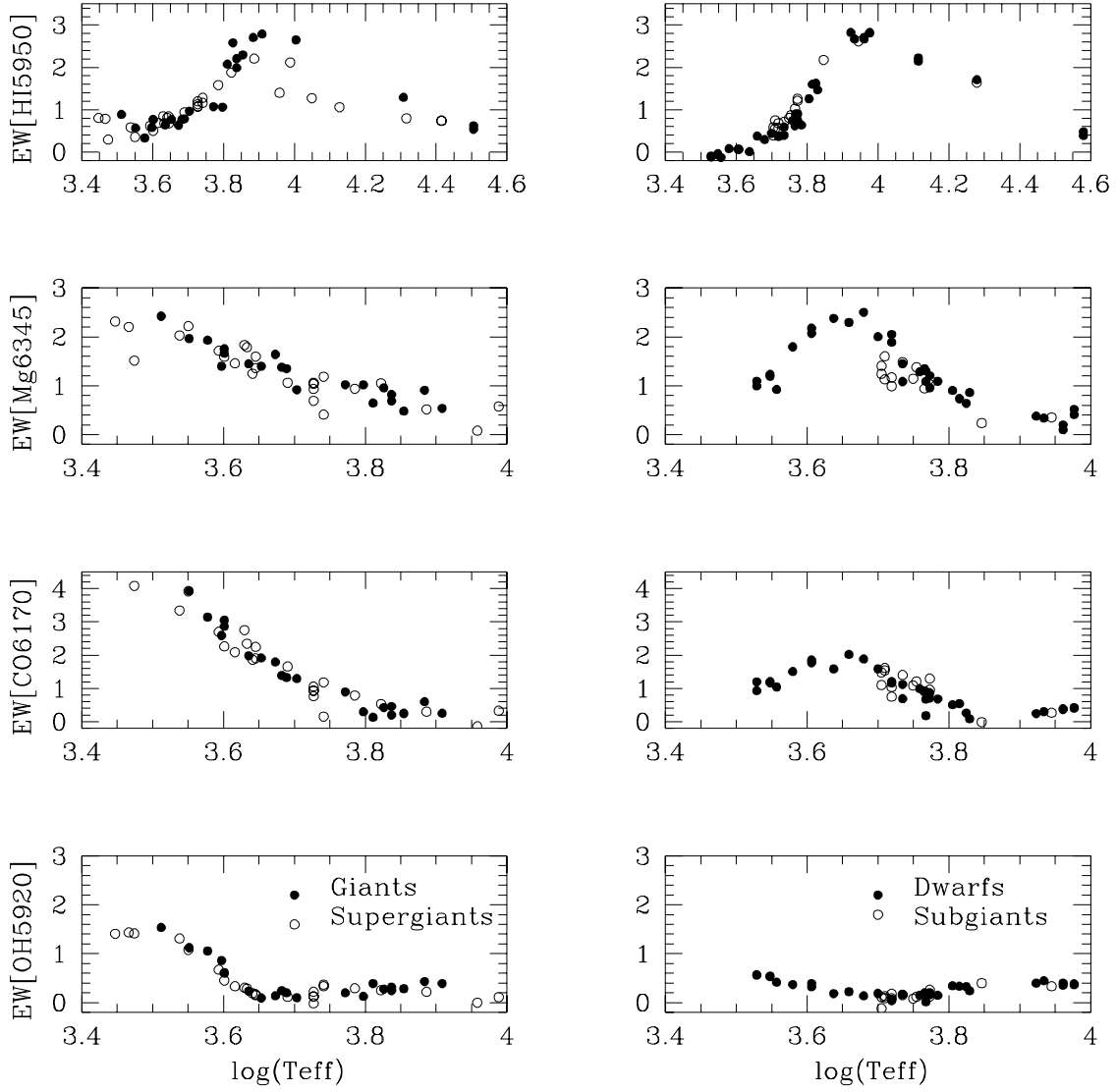


Fig. 7.— Equivalent width of several species listed in Table 4 plotted as a function of effective temperature for stars of high (right panel) and low (left panel) surface gravity. Typical errors are  $< 0.1 \text{ cm}^{-1}$ .

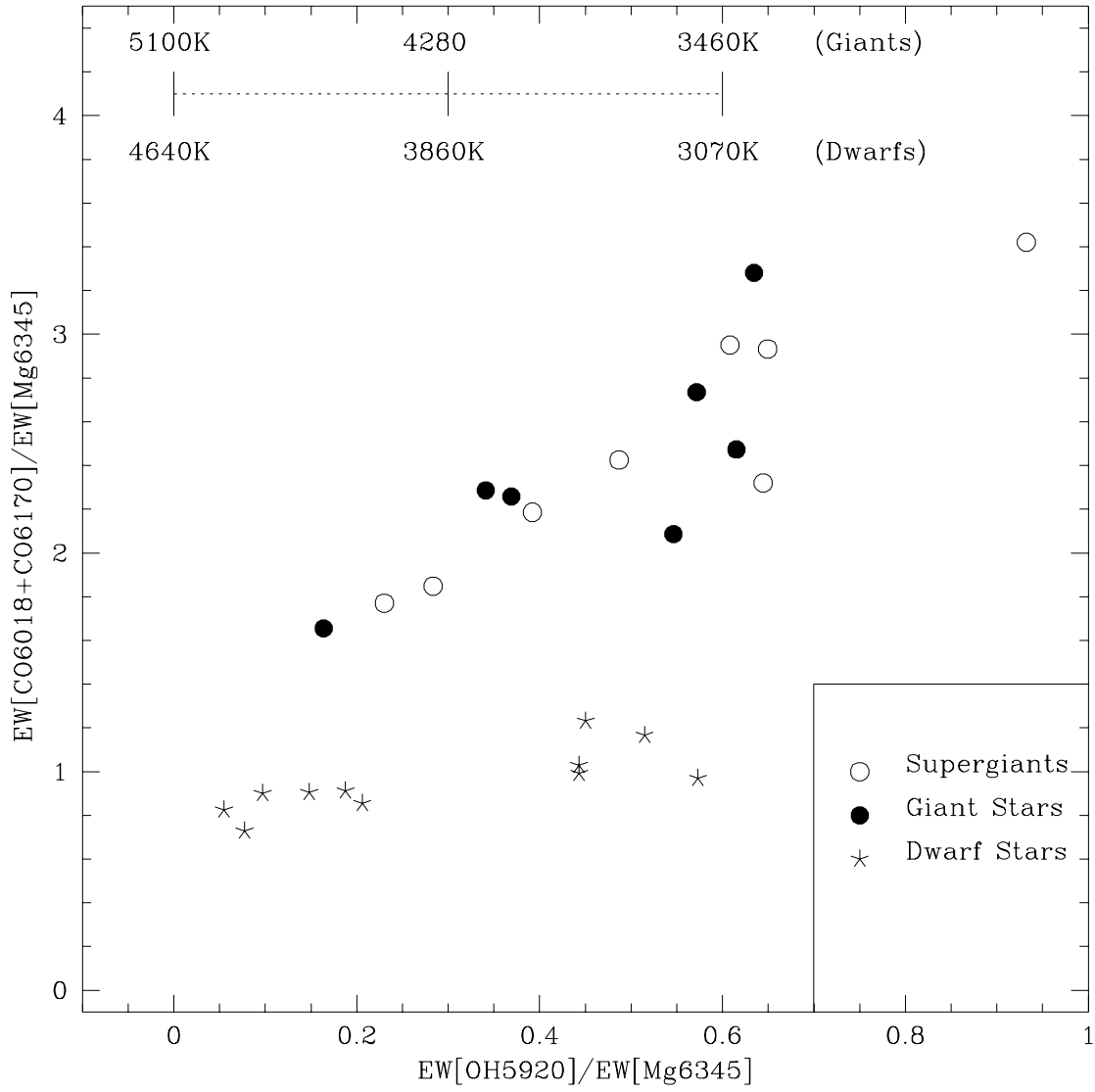


Fig. 8.— Two-dimensional spectral classification for late-type stars K3–M5 using diagnostic line-ratios based on spectra with  $SNR > 50$ . The temperature scales derived for both dwarfs and giants are given.

Table 1: H–Band Survey Sample

HR #	NAME <sup>a</sup>	$m_H$ <sup>b</sup>	ST	Class	RV (km s <sup>-1</sup> ) <sup>c</sup>	vsini (km s <sup>-1</sup> )
1903	*46 $\epsilon$ Ori	2.4	B0	Ia	26SB	87
1203	44 $\zeta$ Per	3.4	B1	Ib	20SB	59
2827	31 $\eta$ CMa	2.5	B5	Ia	41V	45
1713	*19 $\beta$ Ori	0.1	B8	Ia	21SB	33
3975	*30 $\eta$ Leo	3.3	A0	Ib	3V	20
7924	*50 $\alpha$ Cyg	1.0	A2	Ia	-5SBO	21
1865	11 $\alpha$ Lep	2.0	F0	Ib	24	13
1017	*33 $\alpha$ Per	0.9	F5	Ib	-2V	18
7796	*37 $\gamma$ Cyg	1.1	F8	Ib	-8V	20
8232	*22 $\beta$ Aqr	1.5	G0	Ib	7V?	18
7479	5 $\alpha$ Sge	2.4	G1	II	2V?	0
7063	$\beta$ Sct	2.2	G4	IIa	-22SB10	10
8752	* <sub>-</sub>	3.6	G4v	> I <sup>d</sup>	-58V?	35
7314	*21 $\theta$ Lyr	2.1	K0	+II	-31V	<19
6713	93 Her	2.4	K0.5	IIb	-24	<17
8465	*21 $\zeta$ Cep	1.1	K1.5	Ib	-18SB	<17
6498	49 $\sigma$ Oph	1.9	K2	II	-27	<19
603	57 $\gamma^1$ And	-0.5	K3	-IIb	-12SB	<17
8089	*63 Cyg	1.5	K4	Ib-IIa	-26V	-
8079	*62 $\xi$ Cyg	0.5	K4.5	Ib-II	-20SB	<17
2061	58 $\alpha$ Ori	-2.?	M1-2	Ia-Iab	21SB	-
1155	* <sub>-</sub>	0.5	M2	+IIab	-3V	-
921	25 $\rho$ Per	-1.7	M4	II	28	-
7009	* <sub>-</sub>	0.6	M4.5-M5	+II	-19	-
6406	*64 $\alpha^1$ Her	-2.4	M5	Ib-II	-33V	21
1899	44 $\iota$ Ori	3.5	O9	III	22SB2O	130
1552	3 $\pi^4$ Ori	4.1	B2+B2	III	23SBO	40
5291	*11 $\alpha$ Dra	3.5	A0	III	-13SBO	18
403	*37 $\delta$ Cas	2.3	A5	III-IV	7SB	113
1412	*78 $\theta^2$ Tau	2.9	A7	III	40SB1O	78
4031	*36 $\zeta$ Leo	2.8	F0	III	-16SB	84
21	* 11 $\beta$ Cas	1.6	F2	III-IV	12SB	70
5017	*20 CVn	3.9	F3	III	8V?	17
2706	48 Gem	5.0	F5	III-IV	13V	74
8905	*68 $\nu$ Peg	3.3	F8	III	-11	79
4883	*31 Com	3.0	G0	III	-1V?	77
4716	5 CVn	2.8	G6	III	-12SB	<17
7328	1 $\kappa$ Cyg	1.6	G9	III	-29SB	<17
7949	53 $\epsilon$ Cyg	0.2	K0	-III	-11SB?	<17
8317	*11 Cep	2.3	K1	III	-37	<17
6299	*27 $\kappa$ Oph	0.8	K2	III	-56V	<17
165	31 $\delta$ And	0.5	K3	III	-7SB1O	<17
6705	*33 $\gamma$ Dra	-1.2	K5	III	-28	<17
152	-	1.7	K5-M0	III	-33V	<17
4517	*3 $\nu$ Vir	0.3	M1	IIIab	51V?	-
6242	-	0.4	M4	+III-IIIa	-7V?	-
7886	* <sub>-</sub>	-0.6	M6	III	-66V?	-

<sup>a</sup> “\*” indicates that the object also appears in the K–band atlas of WH97.

<sup>b</sup>H–band magnitudes estimated from V–band magnitude from the Bright Star Catalogue, spectral type, and intrinsic colors (Koornneef, 1983).

<sup>c</sup> “V” and “V?” indicate variable or suspected variable radial velocity respectively. “SB1” and “SB2” indicate single– and double–lined spectroscopic binaries respectively. “O” indicates that orbital data is available in the Bright Star Catalogue.



HR #	NAME <sup>a</sup>	$m_H$ <sup>b</sup>	ST	Class	RV (km s <sup>-1</sup> ) <sup>c</sup>	vsini (km s <sup>-1</sup> )
6588	85 $\iota$ Her	4.3	B3	IV	-20SB1O	11
4033	*33 $\lambda$ UMa	3.3	A2	IV	18V	48
1351	57 Tau	4.9	F0	IV	42SB1?	109
5235	8 $\eta$ Boo	1.5	G0	IV	0SB1O	13
5409	105 $\phi$ Vir	2.8	G2	IV	-10SB	0
6623	86 $\mu$ Her	1.4	G5	IV	-16V	20
995	59 Ari	3.9	G6	IV	0V	-
7602	60 $\beta$ Aql	1.7	G8	IV	-40V	< 16
7957	*3 $\eta$ Cep	1.2	K0	IV	-87	<17
5901	11 $\kappa$ CrB	2.5	K1	IVa	-24	<17
6014	-	3.6	K1.5	IV	-4V	-
2456	*15 Mon	5.5	O7	V(e)	33SB	63
5191	*85 $\eta$ UMa <sup>e</sup>	2.4	B3	V	-11SB?	205
3982	*32 $\alpha$ Leo <sup>e</sup>	1.6	B7	V	6SB	329
7001	* $\alpha$ Lyr	0.0	A0	V	-14V	15
2491	*9 $\alpha$ CMa	-1.5	A1	Vm	-8SBO	13
4534	*94 $\beta$ Leo <sup>e</sup>	2.0	A3	V	0V	121
4357	*68 $\delta$ Leo <sup>e</sup>	2.3	A4	V	-20V	181
4931	78 UMa	4.1	F2	V	-10V?	92
1279	-	5.1	F3	V	36SB1?	25
2943	*10 $\alpha$ CMi	-0.6	F5	IV-V	-3SBO	6
1538	59 Eri <sup>e</sup>	2.3	F6	V	35	-
4375	*53 $\xi$ UMa	3.0	G0	V	-16SB1O	1
4983	43 $\beta$ Com	3.1	F9.5	V	6SB?	6
483	*-	3.7	G1.5	V	4V?	2
4374	53 $\xi$ UMa	3.5	G0	V	-16SB1O	3
5072	70 Vir	3.6	G4	V	5V	1
4496	*61 UMa	3.8	G8	V	-5V	<17
7462	*61 $\sigma$ Dra	3.0	K0	V	27V	<17
1084	*18 $\epsilon$ Eri	1.6	K2	V	15V?	<17
8832	*-	3.2	K3	V	-18V	-
-	GL570A	3.0	K4	V	-	-
8085	*61 Cyg	2.4	K5	V	-64V	<17
8086	61 Cyg	3.1	K7	V	-64V?	=<25
-	GL338A	4.5	M0	V	-	-
-	GL526 <sup>f</sup>	4.5	M1.5	V	-	-
-	*GL411	3.6	M2	V	-	-
-	*GL725A	4.7	M3	V	-	-

<sup>d</sup>Previously classified as G0Ia, but it is intrinsically brighter.

<sup>e</sup>Taken from Jaschek, Jaschek, and Condi (1964).

<sup>f</sup>Taken from Henry, Kirkpatrick, and Simons (1994).

Table 2: Temperature Bins for Survey Stars

Spectral Type <sup>a</sup>	$T_{I-II}$ <sup>b</sup>	$T_{III}$ <sup>bc</sup>	$T_{IV-V}$ <sup>b</sup>
O6-O8-	...	37000	38000
O9-	32500	32000	33200
O9.5-	...	...	31450
B0-	26000	29000	29700
B1-	20700	24000	25600
B2-	17800	20300	22300
B3-	15600	17100	19000
B4	13900	...	17200
B5-	13400	15000	15400
B6	12700	14100	14100
B7-	12000	13200	13000
B8-	11200	12400	11800
B9-	10500	11000	10700
A0-	9730	10100	9480
A1-	9230	9480	...
A2	9080	9000	8810
A5-	8510	8100	8160
A7-	...	7650	7930
F0-	7700	7150	7020
F2-	7170	6870	6750
F5-	6640	6470	6530
F7-	...	...	6240
F8-	6100	6150	...
G0-	5510	5910	5930
G2	...	...	5830
G3	4980	...	...
G4	...	5190	5740
G6	...	5050	5620
G8-	4590	4960	...
K0-	4420	4810	5240
K1-	4330	4610	...
K2-	4260	4500	5010
K3-	4130 <sup>d</sup>	4320	...
K4-	...	4080	4560
K5-	3850 <sup>d</sup>	3980	4340
K7	...	...	4040
M0-	3650 <sup>d</sup>	3820	3800
M1-	3550 <sup>d</sup>	3780	3680
M2-	3450 <sup>d</sup>	3710	3530
M3-	3200 <sup>d</sup>	3630	3380
M4-	2980 <sup>d</sup>	3560	3180
M5-	...	3420	3030
M6-	...	3250	2850

<sup>a</sup>“-” denotes full sub-class in the revised MK system. Other full sub-classes for which temperatures are not available without interpolation include B0.5, A3, A8, F3, F9, and G5.

<sup>b</sup>Data taken from Tokunaga, 1996, Astrophysical Quantities, in press.

<sup>c</sup>For giant stars G0 and later data taken from Schmidt-Kaler (1982).

<sup>d</sup>Temperature for star of Luminosity Class Iab.

Table 3: Journal of Observations for the H-Band Survey

Date	Type	# of Stars
March 9–10, 1993	Day	17
April 1–3, 1993	Day/Night	30
May 18–19, 1993	Day	10
January 30–31, 1994	Day/Night	42

Table 4: H-Band Spectral Indices for Classification of A-M Stars

Main Feature <sup>a</sup>	$E_{low}$ (ev)	$\sigma$ (cm <sup>-1</sup> ) <sup>a</sup>	$\lambda$ ( $\mu$ m)	$\sigma_{cent}$ (cm <sup>-1</sup> )	$\Delta\sigma$ (cm <sup>-1</sup> )	Other contr. <sup>a</sup>
MgI(4s–4p)	5.39 <sup>b</sup>	5843.41	1.71133	5844	10	CO, Fe, Ni, OH
OH( $\Delta v = 2$ )	0.76 <sup>c</sup>	5920:	1.689	5920	20	C, CO, Fe, Ni
HI(4-11)	12.75 <sup>d</sup>	5948.50	1.68110	5950	20	CO, Fe, Ni, Si
AlI(4p–4d tr)	4.09 <sup>e</sup>	5963.76	1.67679	5972.5	25	CO, Fe, Ni, OH
		5968.31	1.67552			
		5979.60	1.67235			
SiI(4p–3d)	5.98 <sup>f</sup>	5993.29	1.66853	5993	10	CO, Fe, Ni, OH
<sup>12</sup> CO(8,5)bh	1.55 <sup>g</sup>	6018	1.662	6017.5	15	Fe, OH, S
<sup>12</sup> CO(6,3)bh	1.05 <sup>g</sup>	6177	1.619	6170	50	Ca, Fe, Ni, OH, Si
SiI(4p–5s)	5.98 <sup>f</sup>	6263.92	1.59644	6264	10	Fe, Mg, Ni, OH
MgI(4s–4p tr)	5.93 <sup>b</sup>	6341.10	1.57701	6345	20	CN, CO, Fe, H <sub>2</sub> O, Ni, OH
		6347.88	1.57533			
		6351.22	1.57450			

<sup>a</sup>Species identification and frequencies from LW91 and WL92.

<sup>b</sup>Lower state energy level from Risberg (1965).

<sup>c</sup>Coxon and Forester (1982).

<sup>d</sup>Garcia and Mack (1965).

<sup>e</sup>Eriksson and Isberg (1963).

<sup>f</sup>Litzen (1964).

<sup>g</sup>George, Urban, & LeFloch (1994).

Table 5: Equivalent Widths of Spectral Indices for Luminosity Class I–II Stars

Source	$T_e$	SNR	Mg5844	OH5920	HI5950	Al5973	Si5993	CO6018	CO6170	Si6264	Mg6345
HR1903	26000	203	-0.03	0.09	0.75	0.17	-0.02	0.11	0.27	0.11	0.47
HR1903	26000	167	0.01	0.07	0.73	0.11	-0.00	0.09	0.19	0.12	0.32
HR1203	20700	160	-0.01	0.12	0.80	0.18	0.01	0.11	0.23	0.11	0.56
HR2827	13400	045	-0.05	-0.02	1.06	-0.04	0.20	-0.04	0.01	-0.05	0.08
HR1713	11200	218	0.04	0.06	1.27	0.23	0.05	0.09	0.19	0.17	0.50
HR3975	9730	068	-0.08	0.11	2.12	0.23	0.12	-0.09	0.33	0.20	0.58
HR7924	9080	225	-0.05	0.00	1.40	0.20	-0.02	0.03	-0.14	0.08	0.08
HR1865	7700	196	-0.01	0.22	2.21	0.32	0.14	-0.13	0.30	0.25	0.52
HR1017	6640	248	0.08	0.25	1.88	0.43	0.06	-0.02	0.53	0.41	1.05
HR7796	6100	324	0.10	0.29	1.58	0.69	0.14	0.03	0.79	0.60	0.94
HR8232	5510	290	0.09	0.37	1.28	0.67	0.17	0.03	1.18	0.67	1.19
HR8752	5510	084	-0.13	0.34	1.16	0.14	0.07	0.02	0.16	0.16	0.41
HR7479	5333	096	0.15	0.13	1.13	0.70	0.10	0.00	0.92	0.41	0.69
HR7479	5333	109	0.10	0.22	1.07	0.49	0.11	0.02	0.76	0.54	1.04
HR7479	5333	182	0.13	0.12	1.08	0.56	0.05	0.07	0.94	0.49	1.06
HR7479	5333	093	0.06	-0.02	1.20	0.53	0.03	0.14	1.05	0.54	0.93
HR7063	4902	260	0.17	0.12	0.94	0.84	0.14	0.25	1.66	0.76	1.06
HR7314	4420	193	0.23	0.15	0.84	0.88	0.15	0.46	2.25	1.00	1.60
HR7314	4420	257	0.15	0.17	0.67	0.59	0.10	0.37	1.91	0.86	1.36
HR6713	4375	265	0.22	0.19	0.81	0.80	0.16	0.40	1.86	0.79	1.25
HR8465	4295	308	0.13	0.28	0.68	0.70	0.19	0.63	2.35	1.02	1.79
HR6498	4260	247	0.24	0.30	0.84	1.00	0.21	0.83	2.75	1.11	1.84
HR603	4130	453	0.24	0.34	0.69	0.61	0.19	0.49	2.09	0.87	1.46
HR8089	3990	202	0.21	0.45	0.50	0.67	0.14	0.68	2.26	0.94	1.59
HR8079	3920	445	0.24	0.67	0.62	0.80	0.24	1.05	2.70	1.05	1.72
HR2061	3550	327	0.54	1.08	0.36	1.39	0.23	1.46	3.92	0.89	2.22
HR1155	3450	237	0.46	1.31	0.58	1.12	0.38	1.37	3.35	1.12	2.03
HR921	2980	225	0.77	1.41	0.29	1.27	0.37	1.10	4.08	0.67	1.52
HR7009	2925	292	0.63	1.43	0.79	1.55	0.54	1.79	4.68	1.26	2.21
HR6406	2800	319	0.59	1.41	0.80	1.66	0.54	1.85	4.98	1.31	2.31

Table 6: Equivalent Widths of Spectral Indices for Luminosity Class III Stars

Source	$T_e$	SNR	Mg5844	OH5920	HI5950	Al5973	Si5993	CO6018	CO6170	Si6264	Mg6345
HR1899	32000	164	-0.03	0.17	0.54	0.15	-0.04	0.03	0.18	0.10	0.49
HR1899	32000	182	-0.04	0.20	0.62	0.11	0.05	-0.03	0.07	-0.00	0.07
HR1552	20300	115	-0.07	0.13	1.29	0.31	0.10	-0.09	0.12	-0.01	0.09
HR5291	10100	159	-0.07	0.19	2.65	0.78	0.02	0.05	0.28	0.11	0.41
HR403	8100	202	-0.02	0.39	2.79	0.77	0.09	-0.13	0.25	0.08	0.54
HR1412	7650	186	-0.02	0.43	2.70	0.71	0.05	-0.10	0.60	0.25	0.91
HR4031	7150	193	0.02	0.29	2.30	0.54	0.12	-0.09	0.25	0.13	0.48
HR21	6870	245	0.03	0.32	1.99	0.55	0.04	-0.11	0.20	0.22	0.82
HR21	6870	179	0.01	0.25	2.21	0.63	0.13	-0.14	0.46	0.24	0.69
HR5017	6700	174	0.04	0.28	2.58	0.83	0.07	-0.03	0.43	0.36	0.96
HR2706	6470	086	0.01	0.39	2.08	0.47	0.16	-0.10	0.13	0.20	0.64
HR8905	6270	059	0.06	0.13	1.06	0.45	-0.01	-0.16	0.30	0.28	1.02
HR4883	5910	280	0.15	0.20	1.07	0.52	0.09	0.04	0.90	0.43	1.02
HR4716	5050	133	0.17	0.10	0.97	0.47	0.13	0.07	1.29	0.54	0.92
HR7328	4885	281	0.19	0.20	0.78	0.57	0.11	0.11	1.33	0.67	1.35
HR7949	4810	369	0.21	0.24	0.77	0.59	0.13	0.18	1.39	0.67	1.38
HR8317	4710	191	0.29	0.14	0.63	0.58	0.08	0.26	1.79	0.83	1.64
HR6299	4500	532	0.26	0.09	0.77	0.81	0.10	0.44	1.92	0.76	1.40
HR165	4320	266	0.34	0.24	0.64	0.58	0.18	0.41	1.98	0.89	1.45
HR6705	3990	298	0.39	0.60	0.77	1.12	0.26	0.96	3.05	1.12	1.75
HR6705	3990	694	0.41	0.61	0.76	1.07	0.25	0.89	2.87	1.06	1.66
HR152	3956	270	0.37	0.86	0.58	0.92	0.34	0.87	2.59	0.78	1.40
HR4517	3780	673	0.66	1.06	0.33	1.07	0.21	0.89	3.14	0.70	1.93
HR6242	3560	458	0.52	1.12	0.57	1.18	0.39	1.45	3.93	1.16	1.96
HR7886	3250	574	0.61	1.54	0.89	1.71	0.64	2.25	5.69	1.41	2.42

Table 7: Equivalent Widths of Spectral Indices for Luminosity Class IV Stars

Source	$T_e$	SNR	Mg5844	OH5920	HI5950	Al5973	Si5993	CO6018	CO6170	Si6264	Mg6345
HR6588	19000	162	-0.03	0.10	1.65	0.48	-0.03	0.02	0.17	0.07	0.40
HR4033	8810	146	-0.00	0.33	2.62	0.73	0.06	0.02	0.27	0.13	0.35
HR1351	7020	094	-0.06	0.40	2.18	0.62	0.19	-0.19	-0.01	0.10	0.24
HR5235	5930	341	0.16	0.12	1.21	0.83	0.11	0.03	1.30	0.64	1.14
HR5235	5930	263	0.17	0.26	1.26	0.68	0.18	-0.01	0.97	0.50	1.03
HR5409	5830	158	0.16	0.16	1.02	0.51	0.12	-0.03	0.91	0.44	0.95
HR6623	5680	211	0.33	0.12	0.87	0.87	0.09	0.09	1.21	0.69	1.38
HR995	5620	143	0.22	0.08	0.80	0.61	0.23	0.03	1.09	0.48	1.14
HR7602	5430	056	0.46	0.15	0.71	0.86	0.01	0.17	1.40	0.57	1.49
HR7957	5240	189	0.22	0.09	0.68	0.70	0.07	0.15	1.04	0.46	0.99
HR7957	5240	192	0.09	0.18	0.56	0.52	-0.01	0.09	0.75	0.40	1.17
HR5901	5125	395	0.37	0.13	0.55	0.62	0.08	0.21	1.61	0.74	1.60
HR5901	5125	153	0.37	0.09	0.75	0.93	0.15	0.30	1.54	0.71	1.13
HR6014	5068	072	0.31	-0.12	0.39	0.59	0.14	0.05	1.10	0.70	1.40
HR6014	5068	133	0.42	0.11	0.58	0.55	0.18	0.09	1.48	0.65	1.24

Table 8: Equivalent Widths of Spectral Indices for Luminosity Class V Stars

Source	$T_e$	SNR	Mg5844	OH5920	HI5950	Al5973	Si5993	CO6018	CO6170	Si6264	Mg6345
HR2456	38000	053	-0.03	0.36	0.39	0.26	0.16	0.12	-0.32	0.11	0.31
HR2456	38000	073	-0.12	0.18	0.48	0.10	0.06	-0.15	0.15	0.03	0.10
HR5191	19000	282	-0.05	0.19	1.71	0.57	0.08	-0.07	0.22	0.07	0.24
HR3982	13000	241	-0.08	0.13	2.22	0.47	0.04	-0.09	0.28	0.03	0.15
HR3982	13000	241	-0.07	0.09	2.14	0.51	0.06	-0.09	0.32	0.12	0.26
HR7001	9480	678	-0.05	0.36	2.83	1.06	0.03	-0.03	0.41	0.15	0.52
HR7001	9480	146	-0.10	0.38	2.81	1.02	0.10	-0.05	0.43	0.17	0.41
HR2491	9145	111	-0.07	0.36	2.71	0.83	0.16	-0.14	0.37	-0.08	0.10
HR2491	9145	148	-0.14	0.40	2.67	0.93	0.12	-0.13	0.39	0.05	0.20
HR4534	8593	205	-0.04	0.45	2.67	1.01	0.11	-0.12	0.30	0.07	0.34
HR4357	8377	192	-0.05	0.40	2.83	0.96	0.09	-0.12	0.24	0.06	0.38
HR4931	6750	119	0.04	0.24	1.47	0.62	-0.01	-0.06	0.09	0.09	0.86
HR1279	6677	080	0.10	0.32	1.62	0.67	0.15	-0.09	0.26	0.12	0.64
HR2943	6530	327	0.04	0.33	1.60	0.57	0.15	-0.14	0.54	0.27	0.74
HR1538	6385	281	0.06	0.34	1.26	0.53	0.18	-0.11	0.51	0.22	0.90
HR4375	6085	254	0.26	0.15	0.63	0.56	0.15	-0.06	0.68	0.37	1.09
HR4983	5930	123	0.21	0.16	0.75	0.66	0.09	0.04	0.71	0.45	1.20
HR4983	5930	173	0.19	0.21	0.90	0.52	0.19	-0.06	0.87	0.47	0.96
HR483	5855	059	0.24	0.02	0.68	0.29	0.04	-0.17	0.18	0.37	1.09
HR483	5855	079	0.24	0.19	0.90	0.46	0.19	-0.11	0.67	0.48	1.30
HR4374	5830	250	0.28	0.20	0.62	0.63	0.10	-0.01	0.90	0.47	1.35
HR5072	5740	197	0.26	0.15	0.74	0.53	0.16	-0.04	0.99	0.53	1.28
HR4496	5430	105	0.35	0.17	0.59	0.59	0.21	-0.08	1.12	0.61	1.45
HR4496	5430	090	0.31	0.16	0.39	0.50	0.13	-0.04	0.69	0.43	1.08
HR7462	5240	131	0.52	0.04	0.38	0.72	0.09	0.09	1.20	0.62	1.89
HR7462	5240	095	0.51	0.07	0.37	0.69	0.13	0.06	1.16	0.72	2.05
HR1084	5010	223	0.61	0.19	0.44	0.74	0.24	-0.01	1.59	0.76	2.00
HR8832	4785	111	0.88	0.14	0.29	1.06	0.17	0.18	1.88	0.90	2.50
GL570A	4560	120	0.90	0.22	0.37	1.13	0.28	0.04	2.02	0.90	2.29
HR8085	4340	125	0.65	0.18	0.01	1.15	0.11	0.15	1.59	0.60	2.38
HR8086	4040	170	0.72	0.39	0.06	1.46	0.14	0.11	1.78	0.50	2.07
HR8086	4040	181	0.72	0.32	0.07	1.48	0.15	0.12	1.86	0.52	2.18
GL338A	3800	072	0.98	0.37	0.08	1.36	0.13	0.02	1.51	0.34	1.80
GL526	3605	068	0.62	0.42	-0.13	1.32	0.16	0.10	1.04	0.04	0.92
GL411	3530	202	0.48	0.53	-0.04	1.29	0.16	0.01	1.17	0.10	1.19
GL411	3530	189	0.47	0.55	-0.07	1.29	0.18	0.06	1.21	0.12	1.23
GL725A	3380	083	0.52	0.57	-0.10	1.15	0.06	0.03	0.93	-0.00	0.99
GL725A	3380	107	0.54	0.56	-0.12	1.25	0.02	0.08	1.20	-0.02	1.09